



Cite this: *New J. Chem.*, 2021, **45**, 5127

# Synthesis of cobalt A<sub>2</sub>B triaryl corroles bearing aldehyde and amide pyridyl groups and their performance in electrocatalytic hydrogen evolution†

Jun-Jia Fang,<sup>a</sup> Jian Lan,<sup>a</sup> Gang Yang,<sup>a</sup> Gao-Qing Yuan,<sup>id a</sup> Hai-Yang Liu<sup>id \*a</sup> and Li-Ping Si<sup>\*b</sup>

Four A<sub>2</sub>B type cobalt triaryl corrole complexes (**1–4**) bearing aldehyde and pyridyl substituents at the 10-*meso*-phenyl group with different spatial configurations have been synthesized and thoroughly characterized using high-resolution mass spectrometry, nuclear magnetic resonance spectroscopy (NMR), X-ray photoelectron spectroscopy, and single-crystal X-ray diffractometry. These complexes all exhibited good activity in the electrocatalytic hydrogen evolution reaction (HER) when acetic acid, trifluoroacetic acid (TFA) or *p*-toluenesulfonic acid (TsOH) was used as the proton source. The Tafel catalytic plot revealed the intrinsic characteristics of the catalytic activity. The HER followed the ECEC pathway when acetic acid was used as a proton source, while it proceeded through the EECC or EECEC pathway when using TFA or TsOH as the proton source, depending on the acid concentration. The presence of Co<sup>III</sup>-H was detected by <sup>1</sup>H NMR, which provided evidence for the catalytic mechanism. The amide pyridyl may function as the proton relay group since the *meta*-substituted cobalt corroles **3** and **4** exhibited significantly higher turnover frequency (TOF)<sub>max</sub> values than corroles **1** and **2** in an organic medium.

Received 8th October 2020,  
 Accepted 12th February 2021

DOI: 10.1039/d0nj04953k

rsc.li/njc

## Introduction

Due to the ever-increasing consumption of fossil fuels, the global need for sustainable and environmentally friendly energy has become an enormously concerning topic.<sup>1</sup> Hydrogen, the cleanest fuel, can be obtained by catalytic water splitting.<sup>2</sup> Platinum is one of the most efficient catalysts for the hydrogen evolution reaction (HER). However, its application is seriously limited due to its earth-scarcity.<sup>3</sup> Therefore earth-abundant metals such as cobalt, iron and nickel are in great demand for molecular HER catalysts.<sup>4</sup>

In nature, the reduction of protons can be efficiently achieved by hydrogenase, which is typically found in anaerobic organisms and can convert the protons of water into hydrogen. The amine group positioned near the [Fe-Fe] hydrogenase iron center has been recognized to facilitate the formation of hydrogen *via* proton relay.<sup>5</sup> It has been demonstrated that

cobalt<sup>6</sup> and nickel<sup>7</sup> complexes with pendant amine groups exhibit more effective HER catalytic activity. The pendant amines may accelerate proton transfer between the solution and the active metal site by minimizing the energy barrier of proton transfer, which is helpful for the HER.<sup>8</sup>

It is well known that metal porphyrin complexes have good activity in electrocatalytic hydrogen evolution.<sup>9–11</sup> Corrole is an analogue of porphyrin and can stabilize metal centers with higher oxidation states. As early as 2013, Gross used cobalt tris-pentafluorophenyl corrole as a HER electrochemical catalyst.<sup>12</sup> It was found that electro-withdrawing substituents were beneficial for the HER. The more electron-deficient fluorinated corrole Co-F<sub>8</sub> was found to have better activity than chlorinated or brominated cobalt corroles.<sup>13</sup> Cobalt corroles with phosphonic and carboxyl acid pendants also showed improved activity because of the proton-donating properties of the attached groups.<sup>14</sup> Although cobalt corrole has demonstrated promising electrocatalytic HER activity,<sup>15–17</sup> the question of how to design a molecular structure to facilitate efficient HER is still not fully resolved. Previously, we have tested the electrocatalytic HER activity of cobalt tris-ethoxycarbonyl corrole<sup>18</sup> and triaryl corroles with pendant pentafluorophenyl and amino-,<sup>19</sup> nitro-,<sup>20</sup> cyano-, and 4-*N,N'*-dimethyl-substituted<sup>21</sup> phenyl groups in aqueous solution, and found that electron-withdrawing corroles have higher turnover frequencies (TOFs). In addition to controlling

<sup>a</sup> Department of Chemistry, The Key Laboratory of Fuel Cell Technology of Guangdong Province, South China University of Technology, Guangzhou 510640, P. R. China. E-mail: chhyliu@scut.edu.cn

<sup>b</sup> School of Materials Science and Energy Engineering, Foshan University, Foshan 528000, P. R. China

† Electronic supplementary information (ESI) available. CCDC 1975880, 1975881, 1951203 and 1975879. For ESI and crystallographic data in CIF or other electronic format see DOI: 10.1039/d0nj04953k

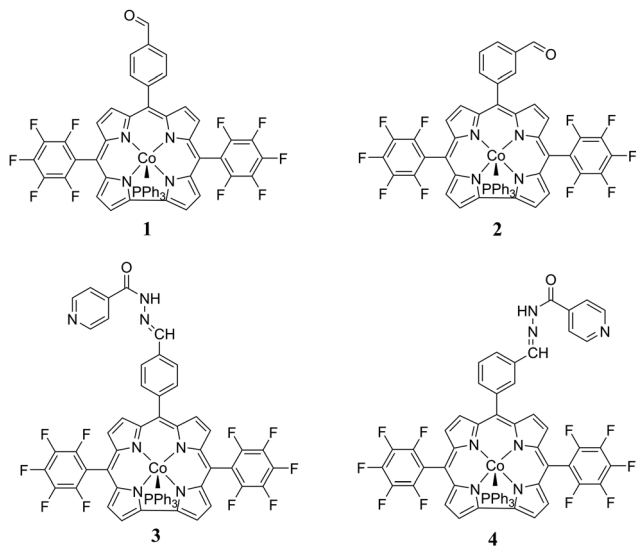


Fig. 1 Molecular structures of the prepared cobalt corroles (1–4).

the push–pull electron density of cobalt corroles, an alternative molecular design idea involves the spatial configuration of the proton relay groups. Bearing this in mind, we herein wish to report the synthesis and electrocatalytic HER activity of a new type of  $A_2B$  cobalt corroles containing pentafluorophenyl and amide pyridyl groups with different spatial arrangements (Fig. 1). When various acids are used as the proton source, corroles 3 and 4 have higher  $\text{TOF}_{\text{max}}$  values than corroles 1 and 2 in pure DMF solution, indicating improved catalytic activity after changing the spatial structures.

## Experimental

### Materials and methods

All reagents were purchased from commercial suppliers and were used without further purification unless otherwise pointed out. UV-Visible spectra were recorded using a Hitachi U-3010 spectrophotometer at room temperature. Nuclear magnetic resonance (NMR) spectra were obtained using a Bruker Avance III 400 MHz or 500 MHz using  $\text{CDCl}_3$ ,  $\text{DMSO}-d_6$  or  $\text{DMF}-d_7$  as the solvent. High-resolution mass spectra (HRMS) were measured using a Bruker Maxis impact mass spectrometer with an electrospray ionization (ESI) source. Cyclic voltammograms (CVs) were performed using a three-electrode system including a Pt wire as the counter electrode, glassy carbon as the working electrode, and  $\text{Ag}/\text{AgNO}_3$  (in DMF) and  $\text{Ag}/\text{AgCl}$  (in acetonitrile/water) as the reference electrodes with a CHI-660E electrochemical analyzer. Ferrocene was added as an internal standard in DMF. The amount of hydrogen after electrolysis was monitored using an Agilent Technologies 7890A GC chromatograph.

### Synthesis of meso-5,15-bis(pentafluorophenyl)-10-(4-formylphenyl)corrole (4-BPFC)

The freebase corrole was synthesized according to a previous report in the literature.<sup>22</sup> Distilled pyrrole (160 mL, 2.30 mol) and pentafluorobenzaldehyde (2.8 g, 14.3 mmol) were added to

a 250 mL dry round-bottom flask along with trifluoroacetic acid (60  $\mu\text{L}$ ). The solution was then stirred at room temperature for an hour, after which triethylamine (120  $\mu\text{L}$ ) was added to neutralize the reaction. The excess pyrrole was removed through vacuum distillation, the product was purified using a column (dichloromethane (DCM)/hexane (HEX) 1/1) and dipyrromethane (DPM) was obtained as a yellow powdered solid (3.6 g, 80.7%). DPM (1.56 g, 5 mmol) and terephthalaldehyde (0.34 g, 2.5 mmol) were dissolved in methanol (250 mL), and then hydrochloric acid (250 mL, 0.6 mol  $\text{L}^{-1}$ ) was added. After being stirred for 1 h, the solution was extracted with DCM. The organic phase was washed with water several times and then dried with  $\text{Na}_2\text{SO}_4$ . Subsequently, 2,3-dicyano-5,6-dichlorobenzoquinone (DDQ) (1.475 g, 6.5 mmol) was added and the solution was stirred for another 20 min. The solvent was then evaporated and the residue was purified using a silica column (DCM/HEX 2/1). The solid was recrystallized by DCM/HEX to obtain the pure violet freebase corrole (0.25 g, 13.9%). MS: (ESI-HRMS)  $m/z$  735.1321  $[\text{M} + \text{H}]^+$ , calculated:  $m/z$  735.1251  $[\text{M} + \text{H}]^+$ .  $^1\text{H}$  NMR ( $\text{CDCl}_3$ , 400 MHz,  $\delta$ , ppm):  $\delta$  10.34 (s, 1H), 9.14 (d,  $J = 12$  Hz, 2H), 8.74 (d,  $J = 4$  Hz, 2H), 8.66 (d,  $J = 4$  Hz, 2H), 8.60 (d,  $J = 4$  Hz, 2H), 8.38 (d,  $J = 8$  Hz, 2H), 8.27 (d,  $J = 8$  Hz, 2H).  $^{19}\text{F}$  NMR ( $\text{CDCl}_3$ , 376 MHz,  $\delta$ , ppm):  $\delta$  -137.82 (4F), -152.50 (2F), -161.58 (4F).  $^{13}\text{C}$  NMR ( $\text{CDCl}_3$ , 101 MHz,  $\delta$ , ppm):  $\delta$  192.33, 147.83, 147.30, 144.87, 142.28, 139.06, 136.65, 135.37, 126.06, 121.58, 117.65, 113.86, 111.85.

### Synthesis of meso-5,15-bis(pentafluorophenyl)-10-(3-formylphenyl)corrole (3-BPFC)

The synthetic route was similar to that of 4-BPFC. MS: (ESI-HRMS)  $m/z$  735.1249  $[\text{M} + \text{H}]^+$ , calculated:  $m/z$  735.1237  $[\text{M} + \text{H}]^+$ .  $^1\text{H}$  NMR ( $\text{CDCl}_3$ , 500 MHz,  $\delta$ , ppm):  $\delta$  10.27 (s, 1H), 9.14 (d,  $J = 4$  Hz, 2H), 8.74 (d,  $J = 4$  Hz, 2H), 8.66 (s, 1H), 8.61 (m, 4H), 8.46 (d,  $J = 8$  Hz, 1H), 8.30 (d,  $J = 8$  Hz, 1H), 7.97 (t,  $J = 8$  Hz, 1H).  $^{19}\text{F}$  NMR ( $\text{CDCl}_3$ , 471 MHz,  $\delta$ , ppm):  $\delta$  -137.72 (4F), -152.58 (2F), -161.52 (4F).  $^{13}\text{C}$  NMR ( $\text{CDCl}_3$ , 126 MHz,  $\delta$ , ppm):  $\delta$  192.47, 147.11, 145.10, 142.44, 140.05, 138.93, 136.99, 135.50, 135.33, 132.73, 128.80, 128.10, 127.41, 125.97, 117.66, 113.93, 111.56.

### Synthesis of meso-5,15-bis(pentafluorophenyl)-10-(4-Schiff-phenyl)corrole (4-BPSC)

4-BPSC (50 mg, 68  $\mu\text{mol}$ ) and isonicotinohydrazide (47 mg, 340  $\mu\text{mol}$ ) were dissolved in methanol (20 mL) and heated to reflux for 24 h. TLC was used to monitor the reaction process, and then the solvent was evaporated and the residue was passed through a silica column (DCM/MeOH 100/1). The solid was recrystallized in DCM and HEX, and a dark violet compound precipitated (35 mg, 60.3%). MS: (ESI-HRMS)  $m/z$  854.1745  $[\text{M} + \text{H}]^+$ , calculated:  $m/z$  854.1721  $[\text{M} + \text{H}]^+$ .  $^1\text{H}$  NMR ( $\text{DMSO}-d_6$ , 500 MHz,  $\delta$ , ppm):  $\delta$  12.32 (s, 1H), 9.22 (s, 2H), 8.97 (s, 2H), 8.85 (t,  $J = 5.5$  Hz, 3H), 8.73 (s, 2H), 8.65 (d,  $J = 3$  Hz, 2H), 8.29 (d,  $J = 6.5$  Hz, 2H), 8.22 (d,  $J = 7$  Hz, 2H), 7.95 (d,  $J = 5.5$  Hz, 2H).  $^{19}\text{F}$  NMR ( $\text{DMSO}-d_6$ , 471 MHz,  $\delta$ , ppm):  $\delta$  -139.57 (4F), -154.78 (2F), -162.88 (4F).  $^{13}\text{C}$  NMR ( $\text{CDCl}_3$ , 126 MHz,  $\delta$ , ppm):  $\delta$  167.46, 162.22, 150.81, 149.97, 149.59, 147.21, 145.32, 143.99, 142.53, 140.64, 139.01, 137.07, 135.57, 133.71, 132.19, 131.95,

129.15, 126.76, 123.78, 122.14, 117.63, 114.28, 65.49, 60.23, 55.32.

#### Synthesis of *meso*-5,15-bis(pentafluorophenyl)-10-(3-Schiff-phenyl) corrole (3-BPSC)

The synthetic method was similar to that of 4-BPSC. MS: (ESI-HRMS)  $m/z$  854.1725 [M + H]<sup>+</sup>, calculated:  $m/z$  854.1721 [M + H]<sup>+</sup>. <sup>1</sup>H NMR (DMSO-*d*<sub>6</sub>, 500 MHz,  $\delta$ , ppm):  $\delta$  12.24 (s, 1H), 9.22 (s, 2H), 8.97 (s, 2H), 8.79 (d,  $J$  = 5.5 Hz, 3H), 8.74 (s, 2H), 8.61 (d,  $J$  = 33.5 Hz, 3H), 8.24 (br, 2H), 7.91 (s, 1H), 7.85 (d,  $J$  = 4 Hz, 2H). <sup>19</sup>F NMR (DMSO-*d*<sub>6</sub>, 471 MHz,  $\delta$ , ppm):  $\delta$  -139.54 (4F), -154.80 (2F), -162.86 (4F). <sup>13</sup>C NMR (CDCl<sub>3</sub>, 126 MHz,  $\delta$ , ppm):  $\delta$  168.39, 162.20, 150.76, 140.71, 139.03, 136.58, 133.70, 128.40, 123.66, 117.71, 114.42, 112.05, 94.49, 72.68, 71.02, 60.71, 60.23, 56.55, 44.09.

#### Synthesis of cobalt *meso*-5,15-bis(pentafluorophenyl)-10-(4-formylphenyl)corrole (1)

The cobalt corrole complexes were synthesized according to a previous report in the literature.<sup>23</sup> A solution of 4-BPFC (100 mg, 136  $\mu$ mol) and Co(OAc)<sub>2</sub>·4H<sub>2</sub>O (169 mg, 680  $\mu$ mol) in methanol (20 mL) was stirred at room temperature, and then triphenylphosphine (178 mg, 680  $\mu$ mol) was added and allowed to react for 2 h. Next, dichloromethane and water were used to extract the organic phase and then passed through a silica column to obtain the pure cobalt *meso*-5,15-bis(pentafluorophenyl)-10-(4-formylphenyl)corrole (1) (75 mg, 52.4%). The synthetic procedure for the other cobalt complexes was similar to that of cobalt corrole 1. MS: (ESI-HRMS)  $m/z$  1053.1239 [M + H]<sup>+</sup>, calculated:  $m/z$  1053.1246 [M + H]<sup>+</sup>. <sup>1</sup>H NMR (CDCl<sub>3</sub>, 500 MHz,  $\delta$ , ppm):  $\delta$  10.29 (s, 1H), 8.77 (d,  $J$  = 4.5 Hz, 2H), 8.29 (d,  $J$  = 4.5 Hz, 2H), 8.23 (t,  $J$  = 4.5 Hz, 3H), 8.15 (t,  $J$  = 10 Hz, 2H), 8.06 (d,  $J$  = 4.5 Hz, 2H), 7.60 (d,  $J$  = 8 Hz, 1H), 7.06 (t,  $J$  = 7.5 Hz, 3H), 6.71 (t,  $J$  = 7.5 Hz, 6H), 4.64 (t,  $J$  = 8 Hz, 6H). <sup>19</sup>F NMR (CDCl<sub>3</sub>, 471 MHz,  $\delta$ , ppm):  $\delta$  -136.86 (4F), -153.87 (2F), -161.79 (4F). <sup>13</sup>C NMR (CDCl<sub>3</sub>, 101 MHz,  $\delta$ , ppm):  $\delta$  192.42, 149.04, 146.12, 144.20, 143.72, 136.10, 135.50, 132.06, 131.45, 131.36, 129.34, 127.23, 126.56, 123.75, 123.26, 122.79, 121.68, 121.08, 115.87, 105.65. <sup>31</sup>P NMR (CDCl<sub>3</sub>, 162 MHz,  $\delta$ , ppm):  $\delta$  26.64 (s, 1P). UV-Vis (*N,N*-dimethylformamide;  $c$ :  $2.8 \times 10^{-5}$  M,  $\lambda_{\text{max}}$ : nm,  $\epsilon$ ; M<sup>-1</sup> cm<sup>-1</sup>): 618 ( $7.74 \times 10^3$ ), 590 ( $6.16 \times 10^3$ ), 568 ( $5.76 \times 10^3$ ), 431 ( $3.38 \times 10^4$ ).

#### Synthesis of cobalt *meso*-5,15-bis(pentafluorophenyl)-10-(3-formylphenyl)corrole (2)

MS: (ESI-HRMS)  $m/z$  1053.1224 [M + H]<sup>+</sup>, calculated:  $m/z$  1053.1246 [M + H]<sup>+</sup>. <sup>1</sup>H NMR (CDCl<sub>3</sub>, 500 MHz,  $\delta$ , ppm):  $\delta$  10.21 (s, 1H), 8.80 (dd,  $J$  = 5.5 Hz, 18.5 Hz, 2H), 8.29 (m, 6H), 8.07 (d,  $J$  = 4.5 Hz, 2H), 7.86 (m, 2H), 7.07 (m, 3H), 6.71 (t,  $J$  = 9.5 Hz, 6H), 4.63 (t,  $J$  = 12 Hz, 6H). <sup>19</sup>F NMR (CDCl<sub>3</sub>, 471 MHz,  $\delta$ , ppm):  $\delta$  -136.81 (4F), -153.91 (2F), -161.79 (4F). <sup>13</sup>C NMR (CDCl<sub>3</sub>, 101 MHz,  $\delta$ , ppm):  $\delta$  192.43, 146.13, 144.31, 144.02, 143.46, 139.03, 136.94, 136.16, 135.36, 133.05, 131.47, 129.27, 128.27, 127.14, 126.62, 123.73, 123.25, 122.86, 120.99, 115.94, 105.59. <sup>31</sup>P NMR (CDCl<sub>3</sub>, 162 MHz,  $\delta$ , ppm):  $\delta$  27.04 (s, 1P). UV-Vis (*N,N*-dimethylformamide;  $c$ :  $2.8 \times 10^{-5}$  M,

$\lambda_{\text{max}}$ : nm,  $\epsilon$ ; M<sup>-1</sup> cm<sup>-1</sup>): 618 ( $1.11 \times 10^4$ ), 590 ( $8.93 \times 10^3$ ), 568 ( $7.27 \times 10^3$ ), 431 ( $4.35 \times 10^4$ ).

#### Synthesis of cobalt *meso*-5,15-bis(pentafluorophenyl)-10-(4-Schiff-phenyl) corrole (3)

MS: (ESI-HRMS)  $m/z$  1172.1765 [M + H]<sup>+</sup>, calculated:  $m/z$  1172.1760 [M + H]<sup>+</sup>. <sup>1</sup>H NMR (CDCl<sub>3</sub>, 400 MHz): <sup>1</sup>H NMR (CDCl<sub>3</sub>, 400 MHz)  $\delta$ : 8.71 (s, 4H), 8.00 (br, 7H), 7.65 (m, 2H), 7.55 (m, 1H), 7.45 (m, 2H), 7.05 (br, 3H), 6.69 (br, 6H), 4.61 (br, 6H), 3.76 (m, 2H). <sup>19</sup>F NMR (CDCl<sub>3</sub>, 376 MHz,  $\delta$ , ppm):  $\delta$  -137.82 (4F), -152.50 (2F), -161.58 (4F). <sup>13</sup>C NMR (CDCl<sub>3</sub>, 101 MHz,  $\delta$ , ppm):  $\delta$  132.19, 131.62, 129.66, 127.30, 123.58, 121.01, 90.00, 31.93, 31.51, 30.11, 29.67, 29.34, 29.15, 27.18, 25.53, 24.86, 22.68, 14.09. <sup>31</sup>P NMR (CDCl<sub>3</sub>, 162 MHz,  $\delta$ , ppm):  $\delta$  26.77 (s, 1P). UV-Vis (*N,N*-dimethylformamide;  $c$ :  $3.2 \times 10^{-5}$  M,  $\lambda_{\text{max}}$ : nm,  $\epsilon$ ; M<sup>-1</sup> cm<sup>-1</sup>): 615 ( $7.69 \times 10^3$ ), 587 ( $6.43 \times 10^3$ ), 422 ( $3.06 \times 10^4$ ).

#### Synthesis of cobalt *meso*-5,15-bis(pentafluorophenyl)-10-(3-Schiff-phenyl) corrole (4)

MS: (ESI-HRMS)  $m/z$  1194.1551 [M + Na]<sup>+</sup>, calculated:  $m/z$  1194.1549 [M + Na]<sup>+</sup>. <sup>1</sup>H NMR (CDCl<sub>3</sub>, 400 MHz): <sup>1</sup>H NMR (CDCl<sub>3</sub>, 400 MHz)  $\delta$ : 8.71 (s, 4H), 8.20 (br, 8H), 7.54 (s, 2H), 7.41 (s, 1H), 7.34 (s, 1H), 6.98 (s, 3H), 6.78 (s, 6H), 4.56 (s, 6H), 3.69 (m, 2H). <sup>19</sup>F NMR (CDCl<sub>3</sub>, 376 MHz,  $\delta$ , ppm):  $\delta$  -137.52 (4F), -154.01 (2F), -162.27 (4F). <sup>13</sup>C NMR (CDCl<sub>3</sub>, 101 MHz,  $\delta$ , ppm):  $\delta$  162.60, 145.50, 129.70, 128.63, 127.36, 124.55, 123.50, 119.07, 36.52, 35.01, 34.47, 31.94, 31.46, 30.17, 29.72, 27.27, 24.92, 22.72, 14.15. <sup>31</sup>P NMR (CDCl<sub>3</sub>, 162 MHz,  $\delta$ , ppm): 30.00 (s, 1P). UV-Vis (*N,N*-dimethylformamide;  $c$ :  $3.2 \times 10^{-5}$  M,  $\lambda_{\text{max}}$ : nm,  $\epsilon$ ; M<sup>-1</sup> cm<sup>-1</sup>): 618 ( $7.69 \times 10^3$ ), 591 ( $6.37 \times 10^3$ ), 421 ( $2.93 \times 10^4$ ).

## Results and discussion

### Synthesis and characterization

Four cobalt corrole complexes were synthesized and characterized using NMR spectroscopy and HR-MS (see the ESI,† S1–S8). 4-BPFC was synthesized through the reaction of DPM and terephthalaldehyde in methanol and hydrochloric acid aqueous solution following the synthetic procedure reported by Gross. Based on this synthetic route, we first synthesized 3-BPFC using DPM and isophthalaldehyde under the same solution conditions with a yield of 34%. We also attempted to synthesize the corrole with the aldehyde group at the *ortho* position of the benzene ring. However, despite trying several synthetic routes, the product was not obtained. We then modified 4-BPFC and 3-BPFC through amidation coupling with isonicotinohydrazide in methanol solution. In their <sup>1</sup>H NMR spectra, the peaks of the protons of the triphenylphosphine unit linked to the central cobalt atom moved in the up-field direction ( $\delta$  = 7.06, 3H; 6.71, 6H; and 4.64 ppm, 6H for corrole 1). For cobalt corroles 1 and 2, the aldehyde protons appeared in the downfield region of 10.21–10.29 ppm. After substitution with the amide pyridyl group, the characteristic proton peak

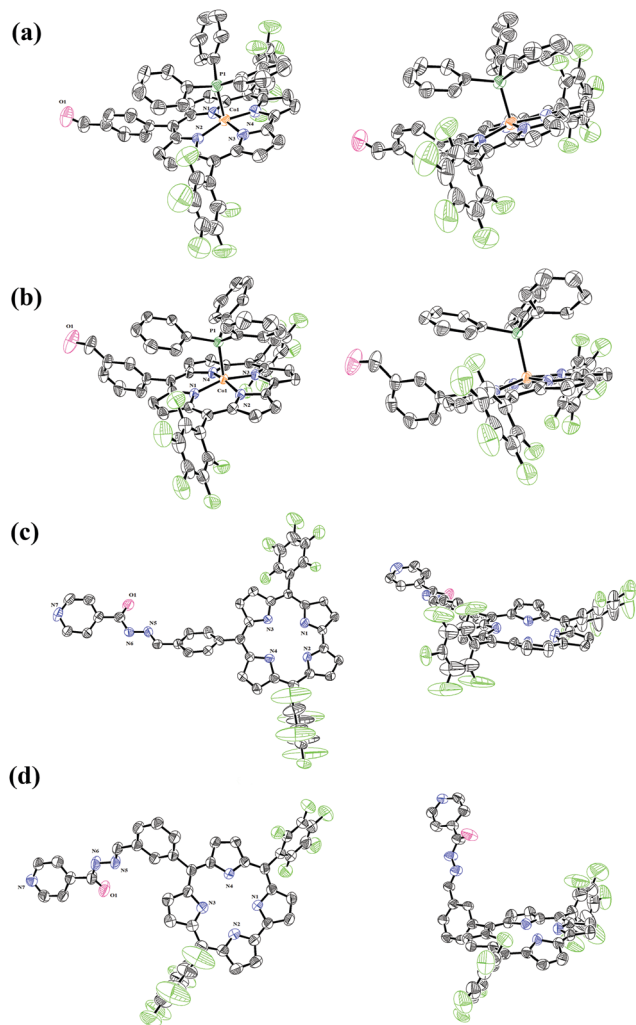


Fig. 2 Thermal ellipsoid plots (50% probability) of the X-ray structures of (a) corrole **1**, (b) corrole **2**, (c) **4-BPSC**, and (d) **3-BPSC**.

disappeared, demonstrating the formation of cobalt corroles **3** and **4**.

We obtained the single-crystal X-ray structures of cobalt corroles **1** and **2**; unfortunately, we observed only the freebase corrole structures of **3** and **4** in the single crystals obtained through the slow evaporation of hexane/dichloromethane mixed solvent, as shown in Fig. 2.

The single-crystal X-ray structures of corroles **1** and **2** showed that the Co ion was coordinated by four N atoms with a PPh<sub>3</sub> group bonded at the axial position. The Co ion deviated from the N<sub>4</sub> plane by 0.3563 Å and 0.4163 Å in corroles **1** and **2**, respectively, due to the steric repulsion from the axial PPh<sub>3</sub> ligand. The distances between the Co and P atoms were 2.2052(16) Å and 2.2088(9) Å, respectively. Furthermore, the average distance of Co–N bond 1.874(4) Å and 1.882(2) Å for corrole **1** and **2** were consistent with a d<sup>6</sup> Co<sup>III</sup> electronic configuration.<sup>24</sup> In the non-metallized corrole structures of **4-BPSC** and **3-BPSC**, the N<sub>4</sub> plane showed less planarity than those of cobalt corroles **1** and **2**. For **4-BPSC**, the planes of the three pyrrole rings were tilted away from the average corrole

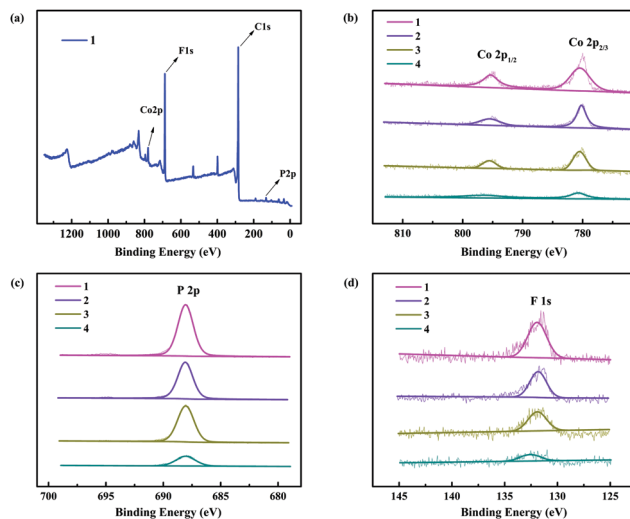


Fig. 3 (a) XPS survey scan spectrum of corrole **1**; (b) XPS Co 2p spectra and (c) P 2p and (d) F 1s binding energy regions of corroles **1**, **2**, **3** and **4**.

plane by 17.192°, 15.266° and 10.470°, while for **3-BPSC**, only one pyrrole ring deviated from the corrole ring plane by 22.905°. The amide and pyridyl groups of **3-BPSC** were relatively closer to the cobalt center than those of **4-BPSC**. Specific crystal data are shown in Tables S1–S4 (ESI<sup>†</sup>). The structures of complexes **1** and **2** and **4-BPSC** and **3-BPSC** have been deposited with the Cambridge Crystallographic Data Center, and their CCDC numbers are 1975880, 1975881, 1951203 and 1975879, respectively.<sup>†</sup>

X-Ray photoelectron spectroscopy (XPS) revealed signals corresponding to Co, F, and P for these cobalt corrole complexes. The XPS survey scan of corrole **1** and the Co 2p, P 2p and F 1s spectra of corroles **1–4** are depicted in Fig. 3. In Fig. 3(b), the peaks of Co 2p<sub>2/3</sub> and Co 2p<sub>1/2</sub> are observed at approximately 780.0 and 795.1 eV, which is consistent with a Co<sup>III</sup> oxidation state.<sup>25</sup> The binding energy of P 2p at 131.6 eV for corrole **1** confirmed the presence of the PPh<sub>3</sub> axial ligand shown in Fig. 3(c). XPS survey scans of corroles **2**, **3** and **4** are provided in Fig. S9 (ESI<sup>†</sup>).

### Electrochemical studies

The electrochemical properties of the cobalt corrole complexes were estimated preliminarily using cyclic voltammetry (CV) in DMF with a complex concentration of 0.83 mM, glassy carbon as the working electrode, 0.1 M TBAP as the supporting electrolyte, Ag/AgNO<sub>3</sub> as the reference electrode and ferrocene as an external standard. The ferrocene redox couple is shown in Fig. S10 (ESI<sup>†</sup>). The potentials in this work are referenced to the ferrocenium/ferrocene (Fc<sup>+</sup>/Fc) couple except when specifically noted. The CVs of these cobalt corrole complexes are shown in Fig. 4. Cobalt corrole complexes **1**, **2**, **3**, and **4** showed irreversible oxidation peaks at 0.28, 0.27, 0.26, and 0.29 V (*E*<sub>pa</sub> versus ferrocene), respectively. The first reduction peaks of the cobalt corroles, which were assigned to Co<sup>III</sup>/Co<sup>II</sup>, appeared at –0.81, –0.83, –0.79, and –0.82 V, respectively. The changes in the spatial structure and electron density led to the differences in the reduction potentials. They are all irreversible due to the

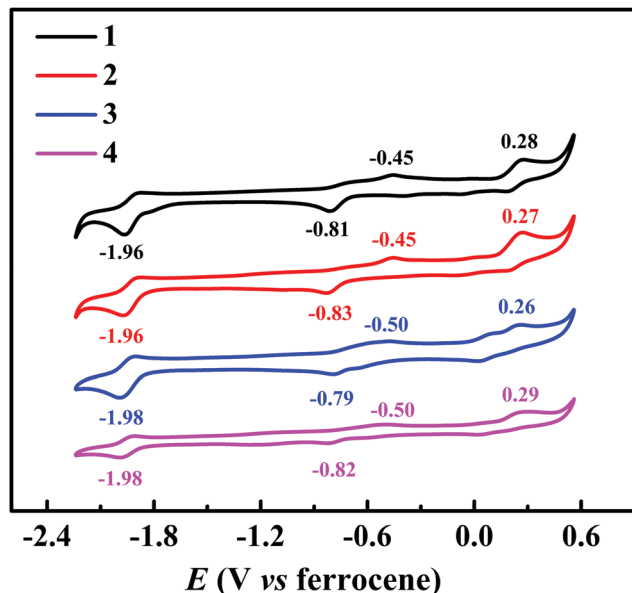


Fig. 4 CVs obtained for complexes **1**, **2**, **3** and **4** (0.83 mM) in DMF containing 0.1 M TBAP as the electrolyte with GC as the working electrode and ferrocene as a reference electrode.

dissociation of the  $\text{-PPh}_3$  ligand.<sup>26</sup> The second reversible redox couples, which were attributed to  $\text{Co}^{\text{II}}/\text{Co}^{\text{I}}$ , were observed at  $-1.96$ ,  $-1.96$ ,  $-1.98$ , and  $-1.98$  V, respectively. All electrochemical values are summarized in Table 1.

The redox peak current of these corrole complexes had a linear relationship with  $\nu^{1/2}$  from 100 to 400  $\text{mV s}^{-1}$ , as shown in Fig. S11 (ESI<sup>†</sup>), which is consistent with the diffusion-limited electron transfer process.<sup>27</sup> The diffusion coefficient  $D$  for the second reduction peak was calculated to be  $1.35 \times 10^{-5}$ ,  $1.41 \times 10^{-5}$ ,  $1.55 \times 10^{-5}$  and  $8.84 \times 10^{-6}$   $\text{cm}^2 \text{s}^{-1}$ , respectively. The  $D$  values were determined using the Randle-Sevcik eqn (1):<sup>28</sup>

$$i_p = 0.4463 n_p F A C_{\text{cat}} \left( \frac{n_p F \nu D}{RT} \right)^{1/2} \quad (1)$$

where  $i_p$  is the peak current,  $n_p$  is the electron stoichiometry,  $F$  is the Faraday constant,  $\nu$  is the sweep rate,  $R$  is the ideal gas constant, and  $T$  is the temperature. The diffusion coefficients in this work were nearly the same as those of cobalt corrole complexes reported by our group.<sup>21</sup>

### Proton reduction of acetic acid in DMF

To examine the differences in their catalytic capability and mechanisms, the performance of the complexes in catalyzing

Table 1 Redox potentials of **1–4** from CV measurements

No.	$E_{1/2}$ (V)		$E_{1/2}$ (V)
	Ox I	Red I	
1	0.23	-0.63	-1.92
2	0.23	-0.64	-1.93
3	0.15	-0.64	-1.95
4	0.16	-0.66	-1.95

proton reduction was investigated in DMF using acetic acid ( $\text{AcOH}$ ,  $\text{p}K_{\text{a}} = 13.2$  in DMF<sup>29</sup>), trifluoroacetic acid ( $\text{TFA}$ ,  $\text{p}K_{\text{a}} = 3.5$  in DMF<sup>30</sup>) or *p*-toluenesulfonic acid ( $\text{TsOH}$ ,  $\text{p}K_{\text{a}} = 2.6$  in DMF<sup>29</sup>) as the proton source. As shown in Fig. 5(a), in the case of corrole **1**, with the addition of acetic acid the first reduction peak was almost identical to that of the blank, while the second reduction couple changed obviously, which indicated that the catalytically active species was  $\text{Co}^{\text{I}}$ . In the presence of acetic acid,  $\text{Co}^{\text{I}}$  combined with a proton and formed  $\text{Co}^{\text{III}}\text{-H}$  species. Note that the second reduction peak was still observed, and that the catalytic current increased at more negative potentials, which revealed that  $\text{Co}^{\text{III}}\text{-H}$  needed to be further reduced to release hydrogen.<sup>31</sup> Similarly, the CVs of corroles **2**, **3** and **4** were measured under the same solution conditions.

To confirm the existence of  $\text{Co}^{\text{III}}\text{-H}$ , we used  $^1\text{H}$  NMR spectroscopy to monitor the formation of the hydride complex (see below). Furthermore, UV-Vis kinetic spectroscopy was applied to study the reaction process.<sup>32</sup> The UV-vis absorbance changed with the addition of cobaltocene and acid, as shown in Fig. 6. An excess (25 equivalents) of cobaltocene was added to a 0.038 mM DMF solution of the complex to reduce  $\text{Co}^{\text{III}}$  to  $\text{Co}^{\text{I}}$ , and different concentrations of acetic acid were then added. In the UV-Vis spectrum, the absorbance decreased evidently at the moment that acetic acid was added, which indicated the formation of  $\text{Co}^{\text{III}}\text{-H}$ . The  $\text{p}K_{\text{a}}$  value of  $\text{Co}^{\text{III}}\text{-H}$  can be calculated (*vide infra*, kinetic study). The  $i_c$  for 18 equiv. of  $\text{AcOH}$  and the  $i_p$  for 0.83 mM of the corrole complex are displayed in Fig. S12 (ESI<sup>†</sup>). The  $i_c/i_p$  plot is shown in Fig. S13 (ESI<sup>†</sup>). The value linearly increased with the addition of acetic acid at first and then reached a plateau. This might be attributed to the consumption of the catalyst at high acid concentration. Based on experimental data and previous references,<sup>31,33</sup> we suggested a catalytic mechanism for these four complexes when acetic acid was used as the proton source as shown in Scheme 1. (I–II–III–V–VI or EECEC pathway; E: electron, C: charge.)

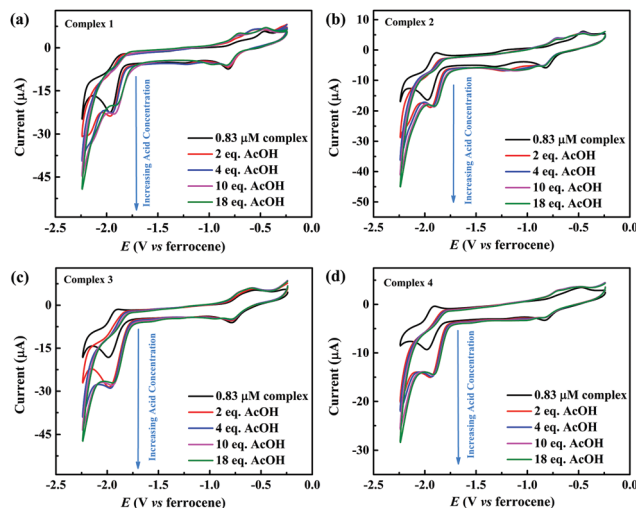


Fig. 5 CVs of corrole complexes (a) **1**, (b) **2**, (c) **3** and (d) **4** (0.83 mM) with the addition of different amounts (0, 2, 4, 10, 18 equiv.) of acetic acid.

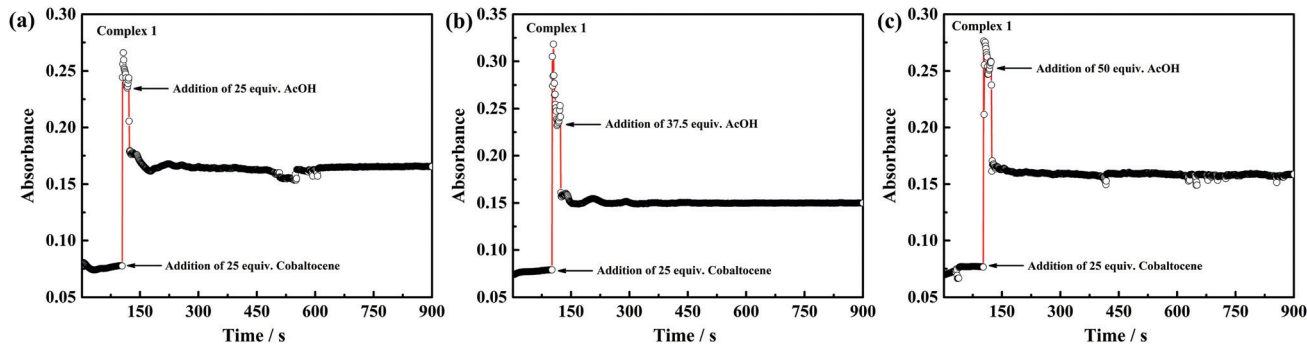
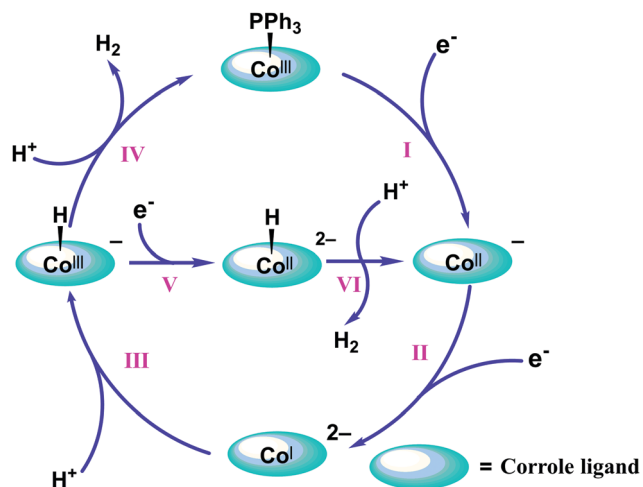


Fig. 6 UV-Vis absorbance of the band at 566 nm after the addition of cobaltocene to corrole **1** in DMF under a nitrogen atmosphere, followed by the addition of (a) 25 equiv., (b) 37.5 equiv. or (c) 50 equiv. acetic acid.



Scheme 1 Possible catalytic cycles of electrocatalytic hydrogen evolution by the cobalt corrole complexes.

### Proton reduction of trifluoroacetic acid (TFA) in DMF

We also examined the catalytic proton reduction performance of the complexes using TFA as the proton source. As shown in Fig. 7, for corroles **1** and **2**, with the addition of TFA, the second reduction peaks became irreversible and the onset potential moved towards the anodic position by approximately 300 and 200 mV. The degree of movement was much greater than that observed for acetic acid. At a TFA concentration of 4.98 mM, two plateaus appeared (magenta line), while at a high concentration of 18.26 mM, the two plateaus merged into one. That indicated that two catalytic mechanisms were involved in the proton reduction process.<sup>31</sup> As can be seen from Fig. 7(a), at the first plateau at  $-1.98$  V,  $\text{Co}^{\text{III}}\text{-H}$  could combine with one proton and release hydrogen (I–II–III–IV or EECC), and the second plateau represented further reduction (I–II–III–V–VI or EECEC). The catalytic mechanisms were the same for the other three corrole complexes. It is noteworthy that cobalt corroles **3** and **4** exhibited two additional waves between  $-1.3$  V and  $-1.7$  V in the presence of TFA and TsOH. These two peaks might be assigned to the reduction of the protonated pyridyl amide group in the stronger acid. In this case, the pyridyl and amide

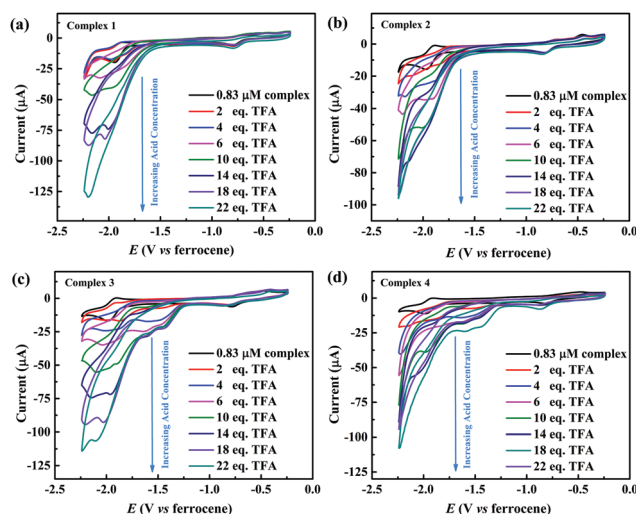


Fig. 7 CVs of complexes of corrole (a) **1**, (b) **2**, (c) **3** and (d) **4** (0.83 mM) in the presence of different amounts (0, 2, 4, 6, 10, 14, 18, 22 equiv.) of TFA.

groups may act as active centers for the HER. A similar phenomenon has also been observed for a catalyst bearing a pendent amine group.<sup>5</sup> The values of  $i_c/i_p$  are presented in Fig. S14 and S15 (ESI<sup>†</sup>).

### Proton reduction of TsOH in DMF

Another strong acid, *p*-toluenesulfonic acid (TsOH), was also used as the proton source. As illustrated in Fig. S16(c) (ESI<sup>†</sup>), after 2 equiv. of acid were added, the first reduction at  $-0.97$  V was almost unchanged, but the second reduction wave became irreversible, implying a proton reduction process. Two peaks appeared at approximately  $-2.2$  V, corresponding to further reduction after the formation of  $\text{Co}^{\text{III}}\text{-H}$ . Similarly to in the case of TFA, the further reduction waves merged into a single peak at  $-2.11$  V at higher acid concentration. Hence, two catalytic pathways proceeded simultaneously. Corroles **1**, **2** and **4** had similar catalytic behavior to corrole **3**. The cobalt-centered and ligand-centered proton reduction processes occurred together. Note that the cobalt-centered catalytic mechanism was dominant, and the catalytic proton reduction route was similar

to that of TFA.<sup>34</sup> The plots of  $i_c$  (in the presence of 22 equiv. TsOH) and  $i_p$  (0.83 mM concentration of cobalt corrole complexes) are shown in Fig. S17 and S18 (ESI†). These results showed that the HER activity of corrole complexes 1–4 was strongly dependent on the acid proton source. Corrole 4 showed the highest  $i_c/i_p$  value among all the tested acids, suggesting that the amide and pyridyl substituents of the corrole may function as proton relay groups to facilitate proton reduction. The values of  $i_c/i_p$  in acetic acid were significantly lower than those in TFA or TsOH. When TFA was used as the proton source, the  $i_c/i_p$  value reached as high as 15, and the maximum TOF of corrole complex 3 was 202.05 s<sup>-1</sup>. In contrast, in TsOH, the maximum TOF of 187.61 s<sup>-1</sup> was achieved by corrole complex 4.

Corrole 1 and 2 and their corresponding freebase forms bear aldehyde groups. To clarify the possibility of reducing the aldehyde to alcohol at the applied negative potentials, we carried out cyclic voltammetry scans for 8 h at a potential of -1.1 V to -1.9 V vs. ferrocene. The FT-IR spectra of these four complexes revealed that the stretching vibration of C=O at approximately 1700 cm<sup>-1</sup> was still present after electrolysis (Fig. S19, ESI†), and no sharp hydroxyl absorption peak corresponding to a primary alcohol was observed near 3640 cm<sup>-1</sup>. This indicated that the aldehyde groups could not be reduced to alcohol at the applied potential. Due to the addition of the electrolyte TBAP to DMF for the electrolysis, strong amide C-H and C-N vibration bands appeared at approximately 3000 cm<sup>-1</sup> and 1090 cm<sup>-1</sup>, respectively.

### Foot of the wave analysis (FOWA) and kinetics study

Upon the addition of TFA or TsOH, the catalytic waves did not follow an S-type plot, so foot-of-the-wave analysis (FOWA) was applied to extract the catalytic kinetic information from the corresponding cyclic voltammograms. FOWA considers only the foot of the wave of the catalytic portion, and thus can eliminate the effects of substrate consumption and deactivation of the catalysts. The catalytic Tafel plots can be derived from the CV and used to analyze the intrinsic properties of the catalyst.<sup>35,36</sup> The TOF follows eqn (2):

$$\text{TOF} = \frac{\text{TOF}_{\max}}{1 + \exp\left[\frac{F}{RT}(E - E_{1/2})\right]} \quad (2)$$

where  $\text{TOF}_{\max} = \frac{k_1 k_2}{k_1 + k_2} C_{\text{subst}}^0$ . Based on the experimental results, we assumed  $k_1 \gg k_2$ , giving us the equation  $\text{TOF}_{\max} = k_2 C_{\text{subst}}^0$ , by introducing the overpotential,  $\eta = E_{\text{H}^+/\text{H}_2}^{\text{ap}} - E$ , where  $C_{\text{subst}}^0$  is the bulk concentration of the species indicated by the subscript and is the overpotential.  $E_{\text{H}^+/\text{H}_2}^{\text{ap}} = E_{\text{H}^+/\text{H}_2}^0 - 0.059 \text{p}K_{\text{a}}$ , where  $E_{\text{H}^+/\text{H}_2}^0 = -1.2$  V vs. ferrocene in DMF and the  $\text{p}K_{\text{a}}$  values of acids are given above.<sup>37</sup> Because the catalytic routes

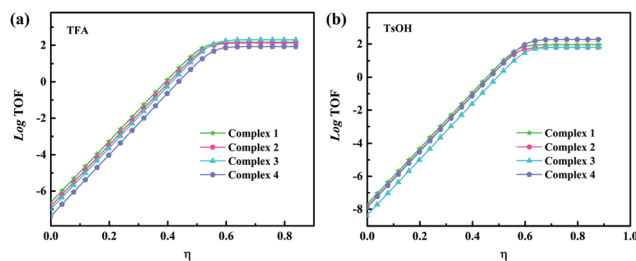


Fig. 8 Catalytic Tafel plots of corrole complexes 1–4 in the presence of TFA and TsOH.

were EECC pathways, eqn (3) was applied,

$$\frac{i}{i_p^0} = \frac{2}{1 + \exp\left[\frac{F}{RT}(E - E_{\text{P/Q}}^0)\right]} \sqrt{\frac{RTk_2}{Fv} C_{\text{subst}}^0} \quad (3)$$

where  $E_{\text{P/Q}}^0$  is the half wave of the catalytic wave obtained from the CV in the absence of acid. In this work,  $E_{\text{P/Q}}^0$  represented the half waves of the second reduction peaks of the cobalt complexes. The slope of  $i/i_p^0$  vs.  $1/1 + \exp[F/RT(E - E_{\text{P/Q}}^0)]$  could be used to calculate  $\text{TOF}_{\max}$  (Fig. S20 and S21, ESI†), and the catalytic Tafel plot is shown in Fig. 8. The  $\text{TOF}_{\max}$  values of these cobalt complexes using TFA and TsOH are summarized in Table 2. The maximum TOFs of corroles 3 and 4 reached 202.05 and 187.61 s<sup>-1</sup> in TFA and TsOH, respectively.

The formation of Co<sup>III</sup>-H was proved to be a key step in the release of hydrogen.<sup>38</sup> In the current system, the existence of a cobalt hydride active species might be proved by <sup>1</sup>H NMR spectroscopy, as shown in Fig. S22 (ESI†). The signals of the active hydrogen of Co<sup>III</sup>-H appeared at around  $\delta = -13$  ppm, and the species was obtained by the addition of two equivalents of cobaltocene and five equivalents of trifluoroacetic acid under a nitrogen atmosphere. The equilibrium constant  $K$  of Co<sup>III</sup>-H was determined using the equation  $\text{Co}^{\text{I}} + \text{H}^+ \rightleftharpoons \text{Co}^{\text{III}}\text{-H}$ , and a kinetic study was carried out *via* UV-Vis spectroscopy based on the absorbance changes *versus* time upon the addition of cobaltocene and acid.<sup>32</sup> As shown in Fig. S23–S27 (ESI†), after the addition of cobaltocene, the absorbance at 566 nm increased significantly, but then decreased after the addition of acetic acid, corresponding to the formation of cobalt hydride. Fig. S28–S30 (ESI†) show the  $\Delta A^{-1}$  vs.  $[\text{AcOH}]^{-1}$  plots used to determine the equilibrium constants  $K$ , and the corresponding  $\text{p}K_{\text{a}}$  values of cobalt hydride in DMF were calculated using eqn (4),

$$\text{p}K_{\text{a}}^{\text{DMF}}(\text{Co}^{\text{III}}\text{-H}) = \text{p}K_{\text{a}}^{\text{DMF}}(\text{Acid}) - \text{p}K \quad (4)$$

Table 2  $\text{TOF}_{\max}$  values of corroles 1–4 in the presence of 22 equiv. of TFA/TsOH

	Corrole 1	Corrole 2	Corrole 3	Corrole 4
$\text{TOF}_{\max}(\text{TFA})$	146.60	134.56	202.05	84.31
$\text{TOF}_{\max}(\text{TsOH})$	90.43	62.17	93.15	187.61

Table 3  $pK_a^{\text{DMF}}(\text{Co}^{\text{III}}-\text{H})$  values of corroles 1–4 in three different acids

$pK_a^{\text{DMF}}(\text{Co}^{\text{III}}-\text{H})$	Corrole 1	Corrole 2	Corrole 3	Corrole 4
AcOH	12.176	10.511	11.716	12.165
TFA	3.024	3.18	2.828	2.978
TsOH	2.333	1.242	2.476	1.826

The  $pK_a^{\text{DMF}}(\text{Co}^{\text{III}}-\text{H})$  values of all the cobalt complexes in the different acids are summarized in Table 3.

### Tafel analysis and charge transfer resistance ( $R_{\text{ct}}$ )

The charge transfer resistance in the organic phase was evaluated using the AC impedance technique. The open circuit potential was set as the fixed potential and the frequency range was 1 MHz to 0.1 Hz. The  $R_{\text{ct}}$  was tested in pure DMF solution containing 0.83 mM of the complex and 18 equiv. AcOH or 22 equiv. TFA/TsOH. The intrinsic resistances ( $R_s$ ) of all four complexes in DMF solution with AcOH were near 1000  $\Omega$ , as shown in Fig. S31 (ESI<sup>†</sup>), while in DMF with TFA (Fig. S32, ESI<sup>†</sup>), the  $R_s$  values of corroles 1–4 were 1188, 563, 876 and 833  $\Omega$ , respectively. Similarly, in DMF with TsOH (Fig. S33, ESI<sup>†</sup>), the  $R_s$  values for corroles 1–4 were 917, 605, 878 and 752  $\Omega$ , respectively. These results suggested that corrole 2 had a higher charge transfer rate and catalytic proton reduction activity than the other three corrole complexes in the presence of TFA and TsOH. Cobalt corrole 4 had a higher charge transfer rate than 3, which may be due to its amide pyridyl groups being closer to the cobalt center, thus benefiting the proton transfer.

The Tafel plots for a 0.83 mM concentration of corroles 1–4 were analysed using the same solution conditions as in the charge transfer resistance ( $R_{\text{ct}}$ ) tests. The anodic and cathodic branches of the Tafel plots were linearly fitted, as shown in Fig. S34–S36 (ESI<sup>†</sup>). The slopes of the red dashed lines ranged from 41 to 60 mV  $\text{dec}^{-1}$  and represented a Heyrovsky step. The blue coloured lines indicated a Volmer step and had slopes between 119 mV and 149 mV  $\text{dec}^{-1}$ .<sup>39</sup>

### Catalyzing hydrogen evolution in an aqueous medium

The three different acids were used as proton sources to evaluate the resulting catalytic abilities of the systems, and the experimental results indicated that this ability was related to their spatial structures. It was obvious that all four cobalt corrole complexes had the ability to catalyze the hydrogen evolution reaction. To evaluate their catalytic performance in an aqueous medium, the controlled potential electrolysis (CPE) technique was used in a mixed neutral medium (acetonitrile/water = 2/3) at different overpotentials. The four corrole complexes were added to the mixed solvent at a concentration of 2.34  $\mu\text{M}$ . To our surprise, with the addition of corrole 1, the charge increased to 111.1 mC with a TOF of 184.3  $\text{h}^{-1}$  at an overpotential of 838 mV, as shown in Fig. 9(a). Similarly, the TOFs of corroles 2, 3, and 4 were calculated to be 171.0  $\text{h}^{-1}$ , 113.6  $\text{h}^{-1}$ , and 129.5  $\text{h}^{-1}$ , respectively, using the relevant equation.<sup>40</sup> The plots of the TOFs and overpotentials of corroles 1–4 are shown in Fig. S37 (ESI<sup>†</sup>). For comparison, the TOFs of other reported first-row transition metal complexes in

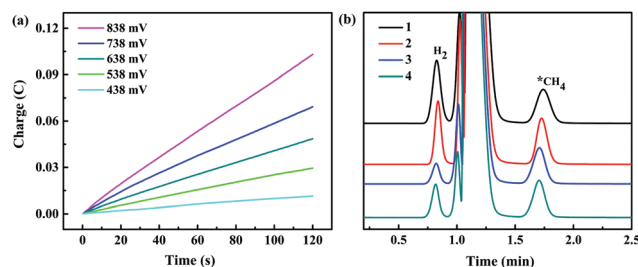


Fig. 9 (a) Charge increase for corrole 1 (2.34  $\mu\text{M}$ ) at different overpotentials. (b) GC traces of corroles 1–4 after 1 h of electrolysis with 0.5 mL  $\text{CH}_4$  as an internal standard.

homogeneous systems are also summarized in Table S5 (ESI<sup>†</sup>). To further investigate the generation of hydrogen, the gas after an hour of electrolysis was analyzed using GC with 0.5 mL methane as an internal standard. As shown in Fig. 9(b), the volumes of hydrogen were 0.637, 0.422, 0.172 and 0.270 mL, which were consistent with the TOFs obtained in the 2 min electrolysis experiment. The hydrogen evolution after electrolysis without any catalyst (bare glassy carbon electrode) and a bare reused electrode under the same conditions were also analyzed using GC (Fig. S38, ESI<sup>†</sup>). No significant difference was observed between the hydrogen production in the systems using the bare fresh and re-used glassy carbon electrode, further demonstrating that the tested cobalt corrole complexes were stable and were not obviously absorbed on the electrode. Corrole 4 had a higher TOF than 3, which indicated that their spatial configurations had an evident effect on their catalytic activity in an aqueous medium. The crystal structures of freebase corroles 3 and 4 showed that the *para*-substituted amide group resulted in obvious distortion of the corrole ring while the *meta*-substituted pyrrole ring had good planarity. The distance between the amide proton relay and the cobalt centre might be one reason for the different catalytic activity. The amide substituents might also participate in intramolecular interactions and the formation of hydrogen bonds due to the arrangement of the corrole ring, which might inhibit the activity of the catalyst.<sup>41</sup> Interestingly, we found that corroles 1 and 2 with an aldehyde-group-substituted benzene ring have higher TOFs than corroles 3 and 4. The detailed catalytic mechanism and the influence of the spatial structures and proton relay transfer on the catalytic activity require further exploration.

### Stability and durability in an aqueous medium

In order to evaluate the stability and durability of the corrole complexes, controlled potential electrolysis (CPE) at a potential of  $-1.25$  V versus NHE was carried out in a neutral 0.25 M phosphate buffer. The current density of these complexes remained nearly unchanged at 5.986, 4.712, 2.318, and 3.218  $\text{mA cm}^{-2}$  for 1, 2, 3, 4, respectively, during the 6 h electrolysis experiment (Fig. S39, ESI<sup>†</sup>). We also examined the UV-vis absorption differences in DMF solution before and after electrolysis, as shown in Fig. S40 (ESI<sup>†</sup>). The spectra were almost the same, which indicated these four catalysts were stable and did not decompose structurally.

## Conclusion

Four A<sub>2</sub>B-type cobalt corrole complexes containing pentafluorophenyl and pyridyl amine groups with different spatial structures have been prepared and thoroughly characterized. The results indicated that the efficiency of proton reduction was closely related to the properties of the acids used. When acetic acid was used as the proton source, the cobalt corrole formed a Co<sup>III</sup>-H intermediate after two-step one-electron reduction; the Co<sup>III</sup>-H was further reduced to a Co<sup>II</sup>-H species and released hydrogen after coupling with a proton (EECEC pathway). When trifluoroacetic or benzenesulfonic acid was used as the proton source, the catalytic process proceeded *via* the EECC pathway at high acid concentration and *via* the EECEC pathway at low acid concentration. The formation of the active species Co<sup>III</sup>-H was detected by <sup>1</sup>H NMR. The values of pK<sub>a</sub><sup>DMF</sup>(Co<sup>III</sup>-H) in different acid environments were explored using UV-Vis kinetic studies. FOWA was used to analyze the intrinsic characteristics of catalytic proton reduction. In the presence of TFA, corrole 3 had the highest TOF<sub>max</sub> of 202.05 s<sup>-1</sup>, and the TOF<sub>max</sub> of corrole 4 reached 187.61 s<sup>-1</sup> in TsOH. These values indicated that the substituted amide pyridyl group was more helpful in catalyzing proton reduction. In neutral aqueous solution, cobalt corrole 4 has a higher TOF than cobalt corrole 3. This implies that the amide pyridyl group may function as a proton relay group. The *meta*-position amide pyridyl is closer to the cobalt center and thus more efficient in facilitating the proton reduction. Interestingly, all four prepared cobalt corroles performed well in the electrocatalytic HER in neutral aqueous solution, and the TOF of cobalt corrole 1 could even reach as high as 184.3 h<sup>-1</sup>. We suggest that the aldehyde group may also act as an inter- or intramolecular proton relay group in aqueous solution. Further investigations along this line are still ongoing in our laboratory.

## Conflicts of interest

There are no conflicts to declare.

## Acknowledgements

This work was supported by the National Natural Science Foundation of China (NNSFC) (No. 21671068 and 22005052).

## Notes and references

- M. J. Rose, H. B. Gray and J. R. Winkler, *J. Am. Chem. Soc.*, 2012, **134**, 8310–8313.
- Y. P. Zhang, M. Zhang, X. R. Chen, C. Lu, D. J. Young, Z. G. Ren and J. P. Lang, *Inorg. Chem.*, 2020, **59**, 1038–1045.
- J. L. Dempsey, B. S. Brunschwig, J. R. Winkler and H. B. Gray, *Acc. Chem. Res.*, 2009, **42**, 1995–2004.
- W. Zhang, W. Lai and R. Cao, *Chem. Rev.*, 2017, **117**, 3717–3797.
- M. L. Helm, M. P. Stewart, R. M. Bullock, M. R. DuBois and D. L. DuBois, *Science*, 2011, **333**, 863–866.
- G. M. Jacobsen, J. Y. Yang, B. Twamley, A. D. Wilson, R. M. Bullock, M. R. DuBois and D. L. DuBois, *Energy Environ. Sci.*, 2008, **1**, 167–174.
- D. L. DuBois and R. M. Bullock, *Eur. J. Inorg. Chem.*, 2011, 1017–1027.
- A. D. Wilson, R. H. Newell, M. J. McNevin, J. T. Muckerman, M. Rakowski DuBois and D. L. DuBois, *J. Am. Chem. Soc.*, 2006, **128**, 358–366.
- B. B. Beyene, S. B. Mane and C. H. Hung, *Chem. Commun.*, 2015, **51**, 15067–15070.
- D. Sirbu, C. Turta, E. A. Gibson and A. C. Benniston, *Dalton Trans.*, 2015, **44**, 14646–14655.
- Y. Han, H. Fang, H. Jing, H. Sun, H. Lei, W. Lai and R. Cao, *Angew. Chem., Int. Ed.*, 2016, **55**, 5457–5462.
- B. Mondal, K. Sengupta, A. Rana, A. Mahammed, M. Botoshansky, S. G. Dey, Z. Gross and A. Dey, *Inorg. Chem.*, 2013, **52**, 3381–3387.
- A. Mahammed, B. Mondal, A. Rana, A. Dey and Z. Gross, *Chem. Commun.*, 2014, **50**, 2725–2727.
- H. Sun, Y. Han, H. Lei, M. Chen and R. Cao, *Chem. Commun.*, 2017, **53**, 6195–6198.
- J. F. Barata, M. G. Neves, M. A. Faustino, A. C. Tome and J. A. Cavaleiro, *Chem. Rev.*, 2017, **117**, 3192–3253.
- X. Liang, Y. Qiu, X. Zhang and W. Zhu, *Dalton Trans.*, 2020, **49**, 3326–3332.
- Y. J. Niu, M. Z. Li, Q. C. Zhang, W. H. Zhu, J. Mack, G. Pono, T. Nyokong and X. Liang, *Dyes Pigm.*, 2017, **142**, 416–428.
- H. Q. Yuan, H. H. Wang, J. Kandhadi, H. Wang, S. Z. Zhan and H. Y. Liu, *Appl. Organomet. Chem.*, 2017, **31**, e3773.
- Y. Chen, Q. H. Fan, M. S. Hossain, S. Z. Zhan, H. Y. Liu and L. P. Si, *Eur. J. Inorg. Chem.*, 2020, 491–498.
- H. Chen, D. L. Huang, M. S. Hossain, G. T. Luo and H. Y. Liu, *J. Coord. Chem.*, 2019, **72**, 2791–2803.
- H. Lin, M. S. Hossain, S. Z. Zhan, H. Y. Liu and L. P. Si, *Appl. Organomet. Chem.*, 2020, **34**, e5583.
- N. Semenishyn, A. Mahammed and Z. Gross, *Eur. J. Org. Chem.*, 2015, 5079–5083.
- L. T. Huang, A. Ali, H. H. Wang, F. Cheng and H. Y. Liu, *J. Mol. Catal. A: Chem.*, 2017, **426**, 213–222.
- H. Lei, A. Han, F. Li, M. Zhang, Y. Han, P. Du, W. Lai and R. Cao, *Phys. Chem. Chem. Phys.*, 2014, **16**, 1883–1893.
- X. Li, H. Lei, J. Liu, X. Zhao, S. Ding, Z. Zhang, X. Tao, W. Zhang, W. Wang, X. Zheng and R. Cao, *Angew. Chem., Int. Ed.*, 2018, **57**, 15070–15075.
- B. Li, Z. Ou, D. Meng, J. Tang, Y. Fang, R. Liu and K. M. Kadish, *J. Inorg. Biochem.*, 2014, **136**, 130–139.
- V. S. Thoi, H. I. Karunadasa, Y. Surendranath, J. R. Long and C. J. Chang, *Energy Environ. Sci.*, 2012, **5**, 7762–7770.
- A. Kumar, S. S. P. Varshney, A. Paul and S. Jeyaraman, *Dalton Trans.*, 2019, **48**, 11345–11351.
- G. A. N. Felton, R. S. Glass, D. L. Lichtenberger and D. H. Evans, *Inorg. Chem.*, 2006, **45**, 9181–9184.
- E. Ahmad, S. Rai and S. K. Padhi, *Int. J. Hydrogen Energy*, 2019, **44**, 16467–16477.
- N. Wang, H. Lei, Z. Zhang, J. Li, W. Zhang and R. Cao, *Chem. Sci.*, 2019, **10**, 2308–2314.

- 32 S. K. Padhi, E. Ahmad and S. Rai, *Electrochim. Acta*, 2020, **340**, 136000.
- 33 S. C. Marinescu, J. R. Winkler and H. B. Gray, *Proc. Natl. Acad. Sci. U. S. A.*, 2012, **109**, 15127–15131.
- 34 X. Hu, B. S. Brunschwig and J. C. Peters, *J. Am. Chem. Soc.*, 2007, **129**, 8988–8998.
- 35 C. Costentin, S. Drouet, M. Robert and J.-M. Savéant, *J. Am. Chem. Soc.*, 2012, **134**, 11235–11242.
- 36 C. Costentin and J.-M. Savéant, *ChemElectroChem*, 2014, **1**, 1226–1236.
- 37 V. Artero and J. M. Saveant, *Energy Environ. Sci.*, 2014, **7**, 3808–3814.
- 38 S. Mandal, S. Shikano, Y. Yamada, Y.-M. Lee, W. Nam, A. Llobet and S. Fukuzumi, *J. Am. Chem. Soc.*, 2013, **135**, 15294–15297.
- 39 T. Shinagawa, A. T. Garcia-Esparza and K. Takane, *Sci. Rep.*, 2015, **5**, 13801.
- 40 L.-Z. Fu, L.-L. Zhou and S.-Z. Zhan, *Catal. Commun.*, 2015, **70**, 26–29.
- 41 R. Orłowski, M. Tasior, O. Staszewska-Krajewska, L. Dobrzycki, W. Schilf, B. Ventura, M. K. Cyranski and D. T. Gryko, *Chemistry*, 2017, **23**, 10195–10204.